Analysis of uncertainty effects due to microstructural disorder in cellular or porous materials

Jörg Hohe *, Volker Hardenacke

Fraunhofer-Institut für Werkstoffmechanik IWM, Wöhlerstr. 11, 79108 Freiburg, Germany

ABSTRACT

Aim of the present study is an analysis of the effect of microstructural uncertainties on the scatter in the macroscopic material properties of highly porous materials consisting of metallic or other constituents. For the numerical analysis of the uncertainty effects, a probabilistic homogenization scheme is proposed. In contrast to direct Monte-Carlo approaches, the thermomechanical response of a limited number of pre-selected cases throughout the range of possible microstructures is analyzed. Their effective properties are determined by means of an energy based homogenization procedure. In a stochastic evaluation, the results of the individual computations are weighted with the probability of the occurrence of the underlying microstructures. As a result, the probability distributions for the effective properties are obtained. The basic uncertain microstructural properties considered in the investigation are the microstructural geometry and orientation, the local relative density and the local pore size distribution. In an application to an experimental data base from other sources, the approach proves to be accurate and numerically efficient compared to direct Monte-Carlo approaches. Parameter studies reveal that uncertainties in the local relative density are the most important factor leading to scatter in the macroscopic material properties of cellular materials.

© 2012 Elsevier Ltd. All rights reserved.

1. Introduction

Porous media and solid foams with high void volume fraction and thus low relative density gain increasing importance in modern lightweight construction. Their main advantage is their low specific weight attained at a reasonable macroscopic stiffness and strength. Hence, porous solids are a natural choice for all kinds of lightweight application. Furthermore, porous media feature superior energy absorption properties due to their high compressibility and the fact that compression occurs at an approximately constant effective stress level (Gibson and Ashby, 1997). Other advantages of cellular materials are their capability for non-structural functions such as heat exchange, thermal and acoustic insulation or catalytic functions and thus their capability for multi-functional application. On the other hand, one of the main disadvantages is their – in many cases – highly disordered microstructure. The uncertainty of the microstructural geometry and topology leads to distinct uncertainties in the macroscopic material response.

For reasons of numerical efficiency, the numerical analysis of structural components made partially or in total from cellular materials is preferably performed in terms of averaged "effective" properties rather than by detailed models of the microstructure. The effective properties can be determined either experimentally or numerically by means of a homogenization analysis. Since the pioneering study by Gent and Thomas (1963) was published, numerous studies on the theoretical and numerical determination of the effective properties of solid foams and other porous media appeared. Most of the available studies are based on idealized periodic models for the cellular microstructure such as the well-known tetrakaidecahedral Kelvin (Thomson and Kelvin, 1887) foam, the brick-like cell model employed by Gibson and Ashby (1997) or the pentagonal dodecahedron model proposed by Christensen (1987). In a more recent study, Weaire and Phelan (1994) proposed a periodic eight-cell model, which outperforms the classical Kelvin foam with respect to Kelvin's (Thomson and Kelvin, 1887) energetic optimality criterion.

For the analytical and numerical analysis of the effective material properties, the idealized periodic foam models have the advantage to require only limited numerical effort since only a single cell or – as in the case of Weaire and Phelan's (1994) model – a small number of cells needs to be analyzed. On the other hand, although these models in general properly account for most of the essential microstructural effects and thus yield reliable estimates of the average effective material properties, they are not able to recapture any disorder effects and the resulting uncertainty in the macroscopic material response. The analysis of these types of effects

* Corresponding author. Tel.: +49 761 5142 340; fax: +49 761 5142 401.
E-mail address: joerg.hohe@iwm.fraunhofer.de (J. Hohe).

requires the application of stochastic approaches (Huyse and Maes, 2001).

Although stochastic methods are well established in experimental investigations on the effective material response of cellular materials (e.g. Blazy et al., 2004; McCullough et al., 1999; Ramamurty and Paul, 2004), they are still not widely established in theoretical and numerical investigations. Most of the available numerical studies concerned with disorder effects are based on a single or repeated analysis of a large-scale representative volume element with a large number of cells, generated by a Voronoï process or similar method for the random division of space. Roberts and Garboczi (2002) and Shulmeister et al. (1998) as well as van der Burg et al. (1997) found a strong scatter of the effective material properties. In a recent study by the present authors Hardenacke and Hohe (2009) on uncertainty effects in two-dimensional honeycombs, a submodel technique has been proposed, where subsets of a large-scale representative volume element are employed as "testing volume elements". Applying the homogenization procedure to the testing volume elements yields a data base for the possible range of the effective properties which is evaluated by stochastic methods to determine their probability distributions. As an alternative, the use of direct probabilistic models has been proposed. In this context, Fortes and Ashby (1999) employed a model based on the structural response of a single cell strut and the probabilities for its spatial orientation. A more sophisticated model based on a stochastic enhancement of the of the deterministic (Gibson and Ashby, 1997) formulae for the effective foam properties has been provided by Schraad and Harlow (2006). Other approaches of this type are e.g. the Taylor averaging scheme proposed by Cuitiño and Zheng (2003).

For the numerical analysis of large-scale representative volume elements, the results of van der Burg et al. (1997) as well as Kanaun and Tkachenko (2006) indicate that the necessary size of representative volume element might be rather large, in order to be statistically representative, requiring cell numbers in the order of 1000 and beyond. Since the numerical analysis of microstructures of this type requires a rather large effort, approaches based on repeated numerical experiments on small-scale testing volume elements with random microstructure are a promising alternative. Approaches of this type have been used by Gan et al. (2005), Li et al. (2006), Zhu et al. (2000), and Zhu and Windle (2002) as well as by one of the present authors (Hohe and Becker, 2005). All of these studies use Monte-Carlo type simulations, where all microstructures analyzed in the numerical experiments are of equal probability. Despite its simplicity, direct Monte-Carlo approaches have the disadvantage to require a rather large number of numerical experiments in order to provide statistically reliable results not only for the mean and the variance of the effective property – as considered in most of the mentioned studies – but also for the upper and lower tails of the corresponding probability distributions.

In order to predict the effective properties and their probability distributions in a numerically more efficient manner, the present study employs a modified approach of this type. Therefore, a number of small to medium scale testing volume elements for the microstructure is considered. Their microstructure is assumed to be defined by a number of uncertain variables such as the (local) relative density, the variance in the pore size distribution or the orientation of the testing volume element in three-dimensional space. In contrast to the mentioned direct Monte-Carlo simulations, pre-selected cases of the microstructure in terms of pre-defined sets of the uncertain variables are analyzed, which cover the entire range of possible microstructural cases. The results of the individual testing volume element analyses are evaluated by stochastic methods, considering the non-uniform probability of occurrence of the microstructures analyzed. In this context, the author's previous approach (Hohe and Becker, 2005) is extended to the analysis of three-dimensional microstructures together with a refined stochastic analysis in terms of the complete probability distributions for the effective properties instead of the basic stochastic parameters alone. The analysis of pre-selected cases throughout the relevant ranges of the essential microstructural parameters instead of the direct Monte-Carlo simulation employed in the previous study in general requires a lower number of simulations and thus provides a higher numerical efficiency, especially for evaluation of the upper and lower tails of the probability distributions of the effective properties.

2. Probabilistic homogenization

2.1. General energy based procedure

Within the present study, the macroscopic "effective" properties are determined numerically by means of a homogenization analysis. For this purpose, a deterministic, energy based homogenization scheme based directly on Hill's (Bishop and Hill, 1951) lemma is adopted (Hohe and Becker, 2001). The original deterministic concept is extended in order to cover uncertainty effects. As most homogenization schemes, the utilized deterministic homogenization procedure considers a representative volume element Ω^{RVE} for the given microstructure and a similar volume element $\Omega^{\mathrm{RVE}*}$ consisting of the "effective" medium with yet unknown properties (Fig. 1). Provided that the characteristic length l of Ω^{RVE} is much smaller than the characteristic length L of the entire body,

$$L \gg l \gg \mathrm{d}l \tag{1}$$

the consideration of Ω^{RVE} and $\Omega^{\mathrm{RVE}*}$ is sufficient for determination of the effective material properties for the quasi-homogeneous body Ω^*, by which the microstructured body Ω is to be replaced. The material law and the corresponding properties of the effective medium have to be determined such that the behaviour of both volume elements, Ω^{RVE} and $\Omega^{\mathrm{RVE}*}$, is equivalent under any kind of loading conditions on the mesoscopic level.

For the definition of the mesoscopic equivalence of the mechanical response of the two volume elements, different approaches have been proposed in the literature. Adopting Hill's (Bishop and Hill, 1951) lemma, the mechanical response of Ω^{RVE} and $\Omega^{\mathrm{RVE}*}$ is assumed to be mesoscopically equivalent, if the average strain energy density in both volume elements is equal

$$\bar{w} = \frac{1}{V^{\mathrm{RVE}}} \int_{\Omega^{\mathrm{RVE}}} w \, \mathrm{d}V = \frac{1}{V^{\mathrm{RVE}*}} \int_{\Omega^{\mathrm{RVE}*}} w^* \, \mathrm{d}V = \bar{w}^* \tag{2}$$

provided that both volume elements are subjected to a mesoscopically equivalent state of deformation. The deformation of both volume elements is defined to be equivalent, if the volume average

$$\overline{F}_{ij} = \frac{1}{V^{\mathrm{RVE}}} \int_{\Omega^{\mathrm{RVE}}} F_{ij} \, \mathrm{d}V = \frac{1}{V^{\mathrm{RVE}*}} \int_{\Omega^{\mathrm{RVE}*}} F_{ij}^* \, \mathrm{d}V = \overline{F}_{ij}^* \tag{3}$$

of the deformation gradient for both volume elements is equal (Hohe and Becker, 2001, 2005).

The energy based homogenization of the cellular microstructure using Eqs. (2) and (3) requires the identification of an appropriate representative volume element, generation of a corresponding finite element model its deformation according to a prescribed effective deformation gradient $\overline{F}_{ij}$ and the computation of the effective average strain energy density $\bar{w}$. Subsequently, the corresponding effective stress and strain components can be determined from $\overline{F}_{ij}$ and $\bar{w}$ using their definitions on the effective level. Within the present study, the effective Green–Lagrange strain
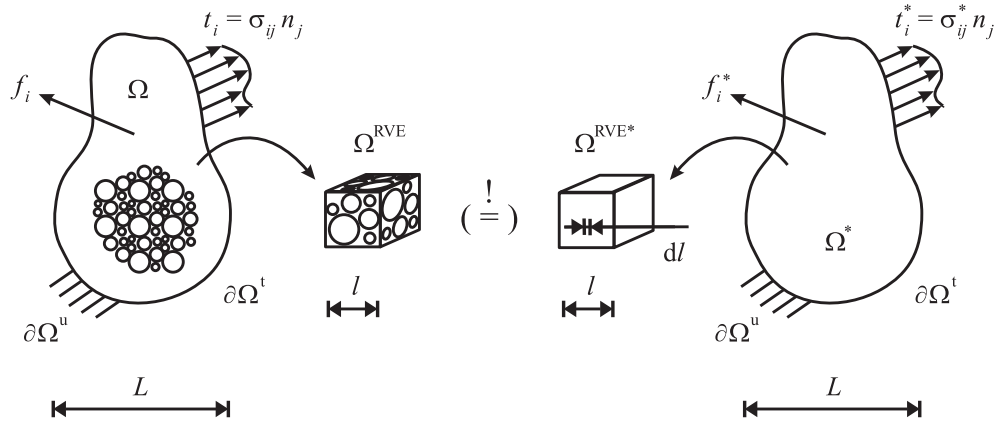
Fig. 1. Concept of the representative volume element.

$$\bar{\gamma}_{ij} = \frac{1}{2}(\bar{F}_{ki}\bar{F}_{kj} - \delta_{ij}) \tag{4}$$

and the effective second Piola-Kirchhoff stress tensor

$$\bar{\tau}_{ij} = \frac{\partial \bar{w}}{\partial \bar{\gamma}_{ij}}\Bigg|_{d\bar{\gamma}_{ij}^{pl}=0} \tag{5}$$

are employed as measures for the effective strain and stress states. Notice that due to the nonlinear dependence of the Green–Lagrange strain tensor on the deformation gradient, the present homogenization scheme does not define the effective strains and stresses as their volume averages. Instead, the deformation components F_{ij} are averaged with respect to the volume element Ω^{RVE}. Assuming periodic microstructures set up by an array of similar volume elements, this definition ensures that the distance between any arbitrary spatial point inside the volume element Ω^{RVE} and a corresponding point in a neighboring volume element is equal in the deformed configuration whether the real microstructure or the effective medium are considered.

Although the energy based homogenization procedure in its original form defined by Eqs. (2) and (3) is restricted to mechanical problems (Hohe and Becker, 2001, 2005), an extension to heat transfer problems is straight forward. For this purpose, the volume elements Ω^{RVE} and Ω^{RVE*} are loaded by prescribed mesoscopic temperature gradients

$$\bar{T}_{,i} = \frac{1}{V^{RVE}} \int_{\Omega^{RVE}} T_{,i} dV = \frac{1}{V^{RVE*}} \int_{\Omega^{RVE*}} T^*_{,i} dV = \bar{T}^*_{,i} \tag{6}$$

for which the volume averages

$$\bar{\dot{q}}_i = \frac{1}{V^{RVE}} \int_{\Omega^{RVE}} \dot{q}_i dV = \frac{1}{V^{RVE*}} \int_{\Omega^{RVE*}} \dot{q}^*_i dV = \bar{\dot{q}}^*_i \tag{7}$$

of the heat flux density have to be equal. Details of the application of the numerical homogenization scheme are given in Section 3.1.

2.2. Probabilistic evaluation

The thermo-mechanical homogenization scheme described in Section 2.1 is basically a deterministic scheme. For a specific microstructure, it enables to determine the effective stress components $\bar{\tau}_{ij}$ corresponding to a prescribed effective strain state $\bar{\gamma}_{ij}$ or, alternatively, the determination of an effective heat flux density $\bar{\dot{q}}_i$ corresponding to an applied effective temperature gradient $\bar{T}_{,i}$. On the other hand, the microstructure of solid foams and other highly porous solids is a stochastic feature involving several constitutive parameters with distinct uncertainties rather than being defined deterministically in the rigorous sense. Important geometric features with uncertainties are the spatial position and the size of

the individual cells. Furthermore, the relative density $\bar{\rho} = (V^{tot} - V^{void})/V^{tot}$ is subject to distinct local uncertainties as it has been shown in experimental studies by Ramamurty and Paul (2004) on ALPORAS foam or in a more recent contribution by Solórzano et al. (2007). Another microstructural constitutive parameter subject to uncertainties is the orientation of the microstructure with respect to the loading direction.

If only the arithmetic averages of the effective material properties are required, the effect of the uncertainties can be accounted for by choosing a large-scale and thus statistically representative volume element. On the other hand, the required size of the volume element in order to be statistically representative might be larger than a characteristic length of the macroscopic structure (Kanaun and Tkachenko, 2006), e.g. if a large-cell solid foam is used as a sandwich core material. Hence, the inequality (1) would be violated and thus no well defined effective properties exist. An alternative to deal with this problem is the application of a stochastic homogenization approach, where the homogenization is performed in a number of repeated numerical experiments using small to medium scale (statistically non representative) testing volume elements. In this case, the results of the individual numerical experiments have to be evaluated by means of stochastic methods.

For this purpose, assume that the microstructure of the testing volume elements is defined by a number of microstructural constitutive variables y such as the relative density $\bar{\rho}$. The actual values of the variables y are uncertain. The uncertainties are described by the probability density distributions $f(y)$ or probability distributions $F(y) = \int_0^y f(y)dy$ can be determined experimentally by a stochastic characterization of the microstructure using tomographic or similar methods. If a number of individual cases of microstructures defined by specific values y_i of the variables y are considered,

$$p(y_i) = \int_{\frac{y_{i-1}+y_i}{2}}^{\frac{y_i+y_{i+1}}{2}} f(y)dy \tag{8}$$

is the individual probability for occurrence of the respective microstructural case considered in the individual testing volume element analysis (Fig. 2). The homogenization results $\bar{Z}(y)$ (e.g. the effective stresses) based on the respective microstructure have the same probability of occurrence as the microstructure itself. Hence, the expectation value $E(\bar{Z}(y))$ and the variance $V(\bar{Z}(y))$ of the effective property $\bar{Z}(y)$ are determined by

$$E(\bar{Z}) = \sum_{i=1}^n \bar{Z}(y_i)p(y_i) \tag{9}$$

$$V(\bar{Z}) = \sum_{i=1}^n (\bar{Z}(y_i) - E(\bar{Z}(y)))^2 p(y_i) \tag{10}$$
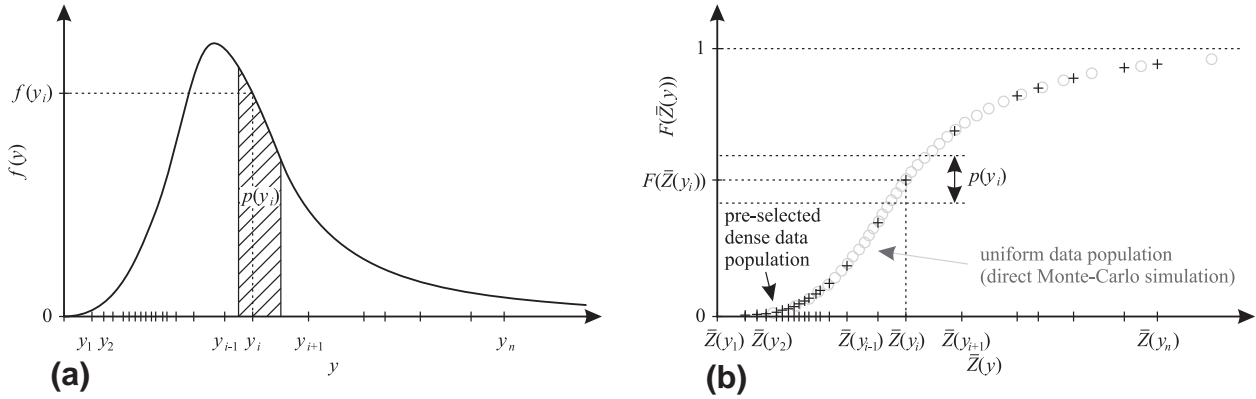
Fig. 2. Probability and probability density of constitutive parameters and effective properties.

as a function of the probability density distribution $f(y)$ for the microstructural constitutive parameter y, where n is the number of numerical experiments. If required, higher order stochastic moments can be determined in a similar manner. For the case that all n microstructures analyzed and thus all homogenization results $\overline{Z}(y_i)$ have the same individual probability $p(y_i) = 1/n$, the direct Monte-Carlo approach as employed in previous studies is recovered (Gan et al., 2005; Hohe and Becker, 2005; Li et al., 2006; Zhu et al., 2000).

With the probabilities $p(y_i)$ of the analyzed microstructures, the probability distribution of the effective property $\overline{Z}(y)$ is obtained by

$$F(\overline{Z}(y_j)) = \sum_{k=1}^{j-1} p(y_k) + \frac{1}{2}p(y_j) \qquad (11)$$

after re-arrangement of the homogenization results $\overline{Z}(y_i)$ into ascending order. The corresponding probability density distribution $f(\overline{Z}(y_j))$ is obtained as the (numerical) derivative of $F(\overline{Z}(y_j))$ with respect to its argument.

In order to avoid difficulties with the numerical determination of the derivative $f(\overline{Z}(y_j))$ of the probability distribution from a limited number of homogenization results, the obtained probability distributions are approximated by a (continuous) logarithmic normal distribution

$$f_{\ln}(\overline{Z}) = \frac{1}{\overline{Z}\sigma(2\pi)^{1/2}} e^{-\frac{(\ln\overline{Z}-\mu)^2}{2\sigma^2}}, \quad F_{\ln}(\overline{Z}) = \int_0^{\overline{Z}} f_{\ln}(\overline{Z})\mathrm{d}\overline{Z} \qquad (12)$$

with the shape and position parameters σ and μ. These parameters are determined from the numerical data in such a manner that the expectation value and the variance

$$E_{\ln}(\overline{Z}) = \int_{-\infty}^{\infty} \overline{Z}f_{\ln}(\overline{Z})\mathrm{d}\overline{Z} = e^{\mu+\frac{\sigma^2}{2}} \qquad (13)$$

$$V_{\ln}(\overline{Z}) = \int_{-\infty}^{\infty} (\overline{Z} - E_{\ln}(\overline{Z}))^2 f_{\ln}(\overline{Z})\mathrm{d}\overline{Z} = e^{2\mu+\sigma^2}(e^{\sigma^2} - 1) \qquad (14)$$

of the computed probability distribution (11) and its approximation (12) are equal. Thus, the basic statistical equivalence of the numerically determined probability distribution and its approximation is guaranteed. If necessary, alternative definitions for the approximated probability distribution may be used. For the problems investigated in the present study, the choice of the logarithmic normal distribution is validated in Section 3.3.

2.3. Application to porous solids

In the present study concerned with porous and cellular solids, brick-shaped testing volume elements are considered. Their microstructure is assumed to contain an identical number of void spheres. The sphere volume is assumed to obey a logarithmic normal distribution (12) with a prescribed shape parameter σ_{csz}. The position parameter μ_{csz} is determined such that the prescribed relative density $\bar{\rho}$ is obtained and thus does not form an independent constitutive parameter. The spheres are positioned randomly into a brick-like testing volume element such that a minimum overlap is achieved. For this purpose, in a preliminary step spheres with a reduced diameter are packed closely into the volume element. Subsequently, the diameter is increased such that the required relative density $\bar{\rho}$ is reached. The microstructures are assumed to be spatially periodic. Hence, if a void sphere intersects with the testing volume element boundaries, the cut-off part of the respective void sphere is added on the opposite side of the testing volume element.

The procedure provides appropriate models for the microstructure of porous solids, replicated foams or microcellular materials. The microstructure is primarily governed by the relative density $\bar{\rho}$ and the shape parameter σ_{csz} of the cell size distribution. In order to account for uncertainties in the microstructural geometry and topology, several testing volume elements are generated for each pair $(\bar{\rho}_i, \sigma_{\mathrm{cszj}})$ of specific values considered for the parameters $\bar{\rho}$ and σ_{csz}. In addition, the orientation of the generated testing volume element relative to the considered loading direction is assumed to be uncertain.

Hence, four different stochastic variables govern the uncertainty in the effective properties of the material considered. The probability for occurrence of the individual homogenization results is given by

$$p = p_{\mathrm{dns}}p_{\mathrm{csz}}p_{\mathrm{ort}}p_{\mathrm{mod}} \qquad (15)$$

where p_{dns}, p_{csz}, p_{ort} and p_{mod} are the individual probabilities for the relative density, the cell size distribution, the spatial orientation and the microstructural geometry respectively. For the basic parameters $\bar{\rho}$ and σ_{csz}, logarithmic normal distributions are assumed, whereas uniform distributions are assumed for all microstructures generated for each pair $(\bar{\rho}_i, \sigma_{\mathrm{cszj}})$ as well as for their spatial orientation. Different types of statistical distributions may be used, if required for any other type of cellular solid.

The main advantage of the proposed scheme compared to a direct Monte-Carlo analysis as employed in previous studies (see Gan et al., 2005; Hohe and Becker, 2005; Li et al., 2006; Zhu et al., 2000) is the possible reduction of numerical effort. Since the considered particular values y_i of the microstructural constitutive parameters y for the individual testing volume elements are pre-selected, areas of particular importance within the total possible ranges of y can easily be provided with a higher density of data points than less important ranges (Fig. 2(b)). Therefore, the spacing of the data points in the accumulated probability distributions $F(y)$

and thus $F(\overline{Z}(y))$ is not necessarily uniform with $p(y_i) = 1/n$, as it would be in a direct Monte-Carlo approach, where the values y_i in the individual numerical experiments would be determined randomly. In a direct Monte-Carlo simulation, the uniform individual probabilities $p(\overline{Z}(y_i))$ would lead to a uniform spacing of the data points in $F(\overline{Z}(y))$-direction (see Fig. 2(b)). Hence, the only possibility to increase the number of data points – and thus the reliability of the probability distribution of the results – in any particular range of the $\overline{Z}(y) - F(\overline{Z}(y))$-diagram is an increase in the total number of simulations. In contrast, the present approach allows a selected increase of the number of data points in particular ranges of the probability distribution such as e.g. the lower tail of the probability distribution in Fig. 2(b). This feature is especially important in analyses of the effective strength or other limit analyses, where the upper or lower bounds of the effective properties rather than their mean values need to be determined. In this case, the scheme proposed in the present study allows the increase in the density of the data points in these regions without the necessity for an increase in the data density in other regions of the probability distribution. Thus, the proposed scheme is in general numerically more efficient than a direct Monte-Carlo simulation, since it requires a fewer number of individual homogenization analyses for achieving a particular data density and thus a particular accuracy of the probability distributions of the effective properties. Alternatively, the accuracy of the results in a particular region of the probability distribution of the effective properties can be increased without increase in the required numerical effort by specifying a higher density of homogenization data in the respective range.

3. Numerical implementation

3.1. Finite element computation

As testing volume elements for the analysis of uncertainty effects in the thermo-mechanical response of porous solids, unit cubes are considered, containing 20 void spheres each. The relative size of the void spheres is described by a logarithmic normal distribution of the type (12) which is defined by the shape parameter σ_{csz}. A vanishing shape parameter $\sigma_{csz} \to 0$ results in a microstructure with uniform cell size whereas increasing σ_{csz} result in microstructures with increasing non-uniformity in the cell size. For analysis of the effective material response, the finite element method is employed. Therefore, the non-void areas of the testing volume elements are meshed with standard displacement based four-node tetrahedral elements. A corresponding temperature based element formulation is employed in the thermal analyses.

In order to cover the entire relevant range for highly porous and foamed materials, relative densities of $\bar{\rho}_i = 0.05, 0.08, 0.11, 0.13, 0.15, 0.17, 0.19, 0.22$ and 0.25 are considered. Five individual shape parameters $\sigma_{cszj} = 0.1, 0.2, 0.3, 0.4$ and 0.5 are analyzed in order to cover the entire range of possible local variations in the cell size distribution. For each pair $(\bar{\rho}_i, \sigma_{cszj})$, five different testing volume elements are generated in order to account for disorder effects caused by the random positioning of the pores. Effects of the spatial orientation of the microstructure are included by an analysis of the model in the orientation as generated as well as in two alternative orientations where the microstructure is rotated by 90° with respect to two different axes x_i of the global Cartesian system.

Examples for the finite element meshes of the random microstructures at different relative densities and different cell size distributions are presented in Fig. 3. The number of nodes in the model varies from 4906 to 14718 whereas the number of elements

ranges from 11664 to 51038. The extreme case of a relative density $\bar{\rho} = 0.25$ constitutes a porous solid with nearly non-intersecting pores. In the lower limit $\bar{\rho} = 0.05$ of the considered density range, microstructures with a rather low relative density are obtained. Due to the limited connection by cell struts between opposite surfaces, low effective stiffnesses will be obtained. In rare cases, even non-percolating microstructures may develop, resulting in a zero stiffness. In the present study, this effect occurs in 12% of the cases for $\bar{\rho} = 0.05$, whereas no such event occurs for all other relative densities. Nevertheless, since all of the homogenization results based on these cases are located in the lower tails of the probability distributions for the effective properties (see Section 4) and thus their individual probability p according to Eq. (15) is almost negligible, no crucial effects develop in the stochastic numerical analysis. Notice that discretized areas in the lower limit $\bar{\rho} = 0.05$ in Fig. 3, which seem to be unconnected to the main discretized body of the microstructure are in general located on the boundaries and thus have a connection to the remainder of the microstructure through the boundary conditions.

The finite element models of the testing volume element are subjected to periodic displacement or temperature boundary conditions. These conditions require that the gradients of the displacement components u_i and the temperature T along the testing volume element surfaces are equal on each pair of corresponding (opposite) surfaces of the unit cube. The discrete boundary conditions for each pair of corresponding nodes on the external testing volume element surfaces are obtained by transforming the volume integrals in the kinematic equivalence conditions (3) or (6) respectively into boundary integrals using Green's theorem. Substituting the periodicity requirements into the results and evaluating the integrals (Hohe and Becker, 2001, 2005) yields

$$\frac{u_i^{(j+)} - u_i^{(j-)}}{l_j} = \overline{F}_{ij} - \delta_{ij} \tag{16}$$

$$\frac{T^{(j+)} - T^{(j-)}}{l_j} = \overline{T}_{,j} \tag{17}$$

where $u_i^{(j+)}$ and $u_i^{(j-)}$ are the displacement components u_i on the testing volume element surfaces with an outward normal unit vector pointing towards the positive and negative x_j-direction, respectively. The temperatures $T^{(j+)}$ and $T^{(j-)}$ are defined in a similar manner. Four additional boundary conditions are required to prevent translatoric rigid body motions and temperature shifts of the testing volume element. Eqs. (16) and (17) allow the direct specification of a prescribed macroscopic state of deformation or macroscopic temperature gradient without evaluation of the integrals in the kinematic equivalence conditions (3) and (6).

The material behaviour on the microscopic level is assumed to be elastic-plastic. The elastic part is governed by Hooke's law whereas J_2-plasticity with polylinear hardening is assumed for the plastic part. In the heat transfer analyses, the linear Fourier heat transfer equation is employed.

3.2. Effective material parameters

For determination of the effective heat transfer properties, the testing volume elements are subjected to an effective temperature gradient $\overline{T}_{,i}$ within the x_i-direction whereas the effective temperature gradients in the remaining spatial directions remain unrestrained. From the finite element analysis, the total heat flux vector $\overline{Q}_i$ through the cross section A_i of the testing volume element is obtained. Subsequently, the effective thermal conductivity

$$\bar{\lambda}_i = -\frac{\dot{\overline{Q}}_{(i)}}{A_{(i)}\overline{T}_{(,i)}} \tag{18}$$

$\bar{\rho} = 0.25$ $\qquad$ $\bar{\rho} = 0.19$ $\qquad$ $\bar{\rho} = 0.15$ $\qquad$ $\bar{\rho} = 0.11$ $\qquad$ $\bar{\rho} = 0.05$
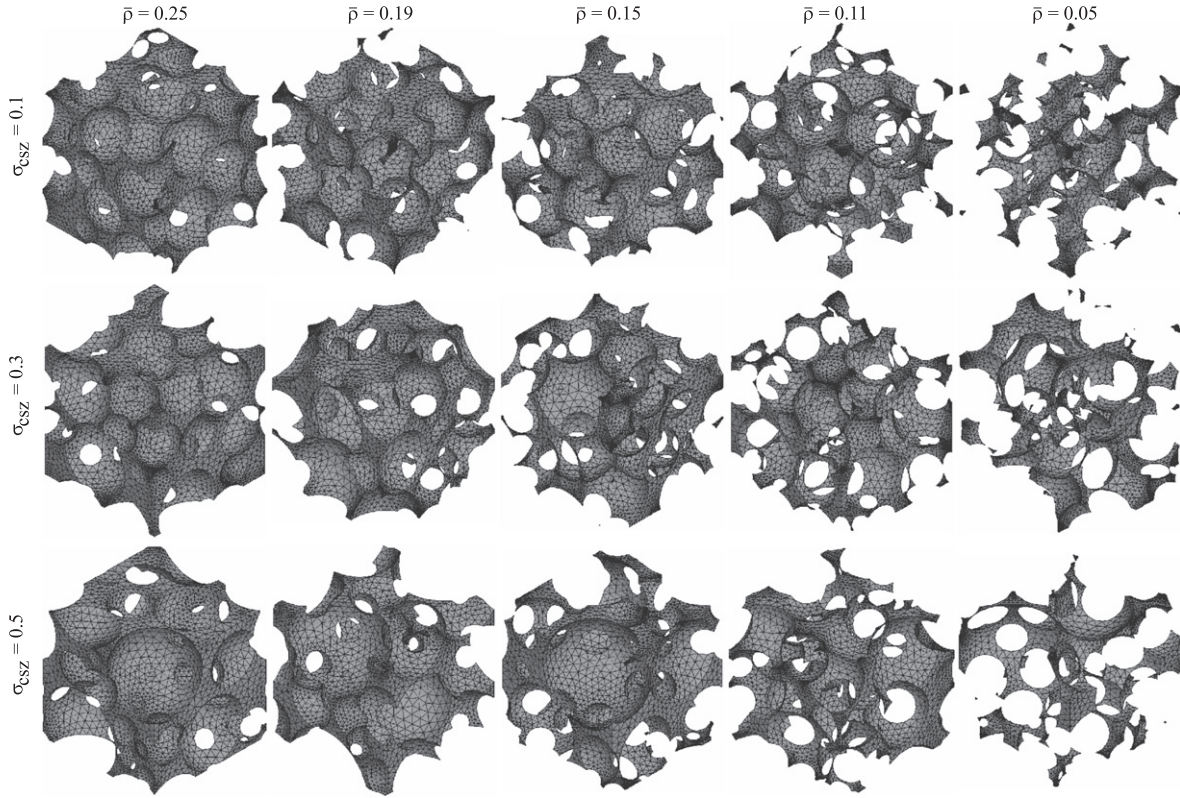

Fig. 3. Examples for the microstructuress of the random testing volume element.

with respect to the x_i-direction can be determined. Embraced indices indicate that no summation is to be performed.

For determination of the elasto-plastic material response on the effective level, the testing volume elements are loaded in a uniaxial manner by a prescribed effective normal strain $\bar{\gamma}_{ij}$ with $j = i$ within the x_i-direction whereas all other effective strain components are left unrestrained. The corresponding components F_{ij} of the deformation gradient are computed by Eq. (4). The prescribed effective normal strain component is increased incrementally into the compressive range. For each increment, the resulting effective stress components are computed resulting in an incremental effective stress-strain curve. For determination of the effective elastic properties, an evaluation increment k_{eval} is chosen, which is the last increment, where the maximum equivalent plastic strain γ_e^{pl} on the microscopic level does not exceed a prescribed small value $\gamma_{e,\text{limit}}^{pl}$. From the effective stress and strain components $\bar{\tau}_{ij}$ and $\bar{\gamma}_{ij}$, the effective elastic constants

$$\bar{E} = \frac{\bar{\tau}_{\text{load}}}{\bar{\gamma}_{\text{load}}} \qquad (19)$$

and

$$\bar{v} \approx -\frac{1}{2} \frac{\bar{\gamma}_{p1} + \bar{\gamma}_{p2}}{\bar{\gamma}_{\text{load}}} \qquad (20)$$

are determined, where $\bar{\tau}_{\text{load}}$ and $\bar{\gamma}_{\text{load}}$ are the effective normal stress and strain components within the actual loading direction whereas $\bar{\gamma}_{p1}$ and $\bar{\gamma}_{p2}$ are the effective normal strain components perpendicular to the macroscopic loading direction.

The effective hardening curve is defined directly as the computed uniaxial effective stress-strain curve, where the effective plastic strain is approximated by

$$\bar{\gamma}_e^{pl} = \bar{\gamma}_{\text{load}} - \frac{\bar{\tau}_{\text{load}}}{\bar{E}} \qquad (21)$$

assuming that the elastic properties do not change significantly during the plastic deformation at least during its initial stage. A macroscopic yield stress $\bar{\tau}_y$ is defined in the sense of an 0.2% offset stress as the effective stress at $\bar{\gamma}_e^{pl} = 0.002$.

By determination of the effective thermal conductivity $\bar{\lambda}$, the effective elastic constants $\bar{E}$ and $\bar{v}$ as well as the effective yield stress $\bar{\tau}_y$ for a variety of relative densities, cell size distributions, microstructural geometries and orientations, a numerical raw data base for the subsequent stochastic evaluation according to Section 2.2 is established. The raw data base is presented in Fig. 4. As a material example for the cell wall material, aluminium with $E_0 = 70$ GPa, $v_0 = 0.3$, $\tau_{y0} = 190$ MPa and $\lambda_0 = 238$ W/(mK) is assumed. Nevertheless, all computed effective material constants are normalized with respect to their microscopic counterparts in order to provide a more general representation. As expected, the effective Young's modulus $\bar{E}$, the effective yield stress $\bar{\tau}_y$ as well as the effective thermal conductivity $\bar{\lambda}$ exhibit a strong dependence on the relative density $\bar{\rho}$. No such effect is observed for the effective Poisson's ratio $\bar{v}$, since this quantity is a mechanism controlled property relying on the underlying microscopic mechanism of deformation rather than on the microscopic material properties. For the cell size distribution of the porous medium, no distinct effect is visible in the raw data presentation in Fig. 4. Both effects will be discussed in detail in the stochastic evaluation of the raw data presented in Section 4.

3.3. Validation

Prior to the application of the probabilistic homogenization approach proposed in Section 2 in parametric studies, the raw data base is validated against experimental results. In Fig. 5, the raw data determined in Section 3.2 are compared with experimental data from different literature resources. In Fig. 5(a), the elastic modulus $\bar{E}$ of the porous material normalized with the Young's
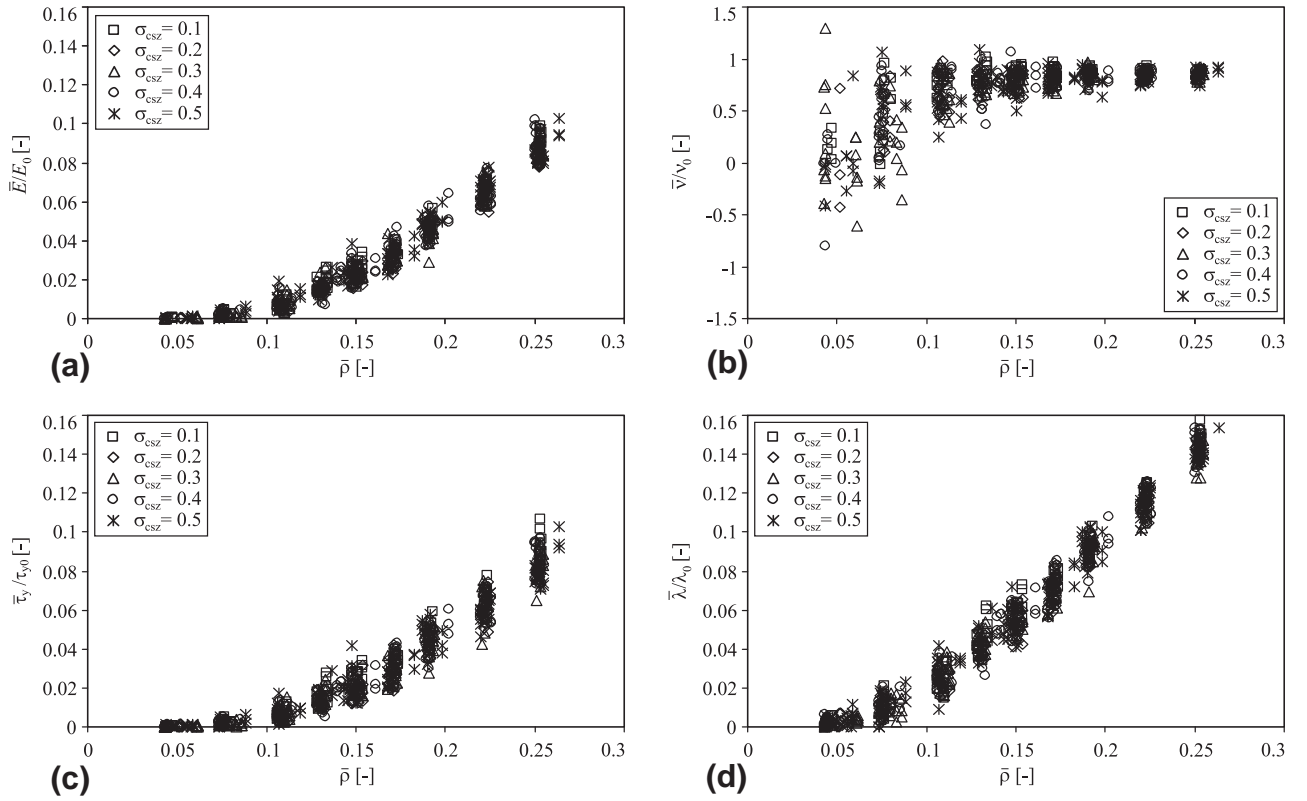
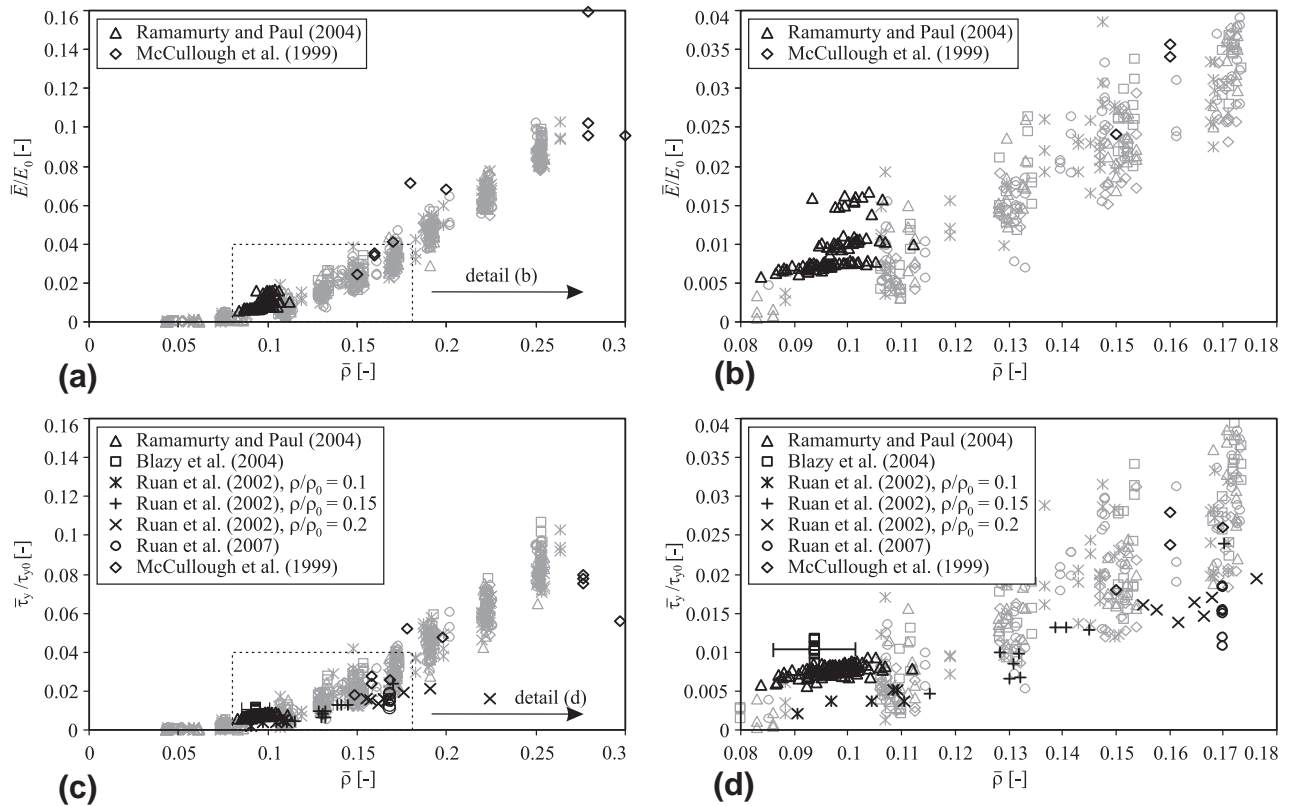**Fig. 4.** Raw data for the normalized effective elastic constants.

Fig. 5. Comparison of the raw data base with experimental data.

modulus E_0 of the cell wall material is plotted as a function of the the relative density $\bar{\rho}$ of the porous solid. Fig. 5(b) shows an enlarged detail of Fig. 5(a). The numerical raw data obtained in the numerical homogenization analysis are found in a rather good agreement with the stochastic experimental measurements provided by Ramamurty and Paul (2004). In this context, the experimental data were re-calculated to the measured data instead of the specimen length normalized data presented by Ramamurty and Paul (2004).

In light of the oncoming stochastic evaluation of the raw data base in Section 4, it should be noticed that the stochastic experimental investigation by Ramamurty and Paul (2004) has been performed on closed cell ALPORAS aluminum foam samples with a nominal relative density of $\bar{\rho} \approx 0.096$. Despite the unique nominal relative density of the plate, where their specimens were cut from, a distinct uncertainty in the relative density of the individual specimens occurs. The scatter in the relative density might become even more distinct, if subsets of the tested specimens would be analyzed.

In comparison to the stochastic approach of Ramamurty and Paul (2004), McCullough et al. (1999) do not provide a rigorous stochastic analysis of their experimental results. On the other hand, their study on density effects in the effective material response of highly porous materials covers a rather wide range of relative densities and therefore provides a good reference for the present numerical raw data. In average, the experimental data of McCullough et al. (1999) are in good agreement with the raw data obtained by the present numerical homogenization analysis. Hence, the accuracy and reliability of the numerical scheme is evident.

For the normalized yield stress $\bar{\tau}_y/\tau_{y0}$, more exhaustive experimental investigations are available in the literature. In addition to the previously considered publications by Ramamurty and Paul (2004) and McCullough et al. (1999), experimental studies by Blazy et al. (2004) as well as by Ruan et al. (2002, 2007) are considered as reference cases for the accuracy of the present numerical raw data base. A comparison of the experimental results with the numerical raw data of the present study is presented in Fig. 5(c) as well as in the enlarged detail in Fig. 5(d). In general, the experimental results are found in a good agreement with the numerical data. Nevertheless, it has to be mentioned that the numerical results obtained in the present study are rigorous 0.2% offset stress values whereas the yield stress in most experimental approaches is defined either as the peak stress preceding the stress plateau in compression or directly as the plateau stress. Especially if taken at larger (macroscopic) compressive effective strain levels, the plateau stress can be linked with an already damaged microstructure and therefore might underestimate the initial yield limit. Hence, the numerical values and experimental results might not be directly comparable in the rigorous sense. Nevertheless, the good qualitative agreement of the experimental results and the numerical raw data again underlines the apropriateness of the numerical raw data base.

In the probabilistic evaluation scheme proposed in Section 2.2, the probability distributions for the effective properties are determined from the raw data base by weighting the individual homogenization results with the probability for occurrence of the underlying microstructure. Subsequently, the numerically determined discrete probability density distribution for the considered property is approximated by a logarithmic normal distribution (12). In Fig. 6, the discrete probability distributions $F(\bar{E}/E_0)$, $F(\bar{v}/v_0)$, $F(\bar{\tau}_y/\tau_{y0})$ and $F(\bar{\lambda}/\lambda_0)$ for the effective elastic constants, the effective yield stress and the effective thermal conductivity are plotted under the assumption of a logarithmic normal distribution of the relative density $\bar{\rho}$ with an expectation value of $E(\bar{\rho}) = 0.15$ and a standard deviation of $\sqrt{V(\bar{\rho})} = 0.02$. In all four cases, an almost perfect coincidence of the numerically computed discrete probability distributions with the continuous

approximation is obtained. For other expectation values and standard deviations of the relative density $\bar{\rho}$, similar results are obtained. Hence, the approximation of the discrete numerical probability distributions by a continuous logarithmic normal distribution for further evaluation purposes is clearly justified.

4. Parametric studies

4.1. Effects of uncertainties in the relative density

In a first parametric study, the effect of the uncertainty in the local relative density $\bar{\rho}$ of the cellular material is studied. Experimental results reported by Ramamurty and Paul (2004) reveal that distinct variations of the relative density around its nominal value might occur for cellular solids even on laboratory specimens size level with a larger characteristic length scale as for the microstructural models considered in the present study. The local variation of the relative density is characterized by a logarithmic normal distribution defined by the expectation value $E(\bar{\rho})$ and the corresponding standard deviation $\sigma(\bar{\rho})$. Five different levels of the standard deviation ranging from $\sigma(\bar{\rho}) = 0.004$ up to 0.02 are considered. The lowest level corresponds to a spatially nearly constant relative density of the material whereas the highest level defines a material with distinct uncertainties in the local relative density. In Fig. 7, the probability distributions $f(\bar{E}/E_0)$, $f(\bar{v}/v_0)$, $f(\bar{\tau}_y/\tau_{y0})$ and $f(\bar{\lambda}/\lambda_0)$ for the effective elastic constants, the effective yield stress and the effective thermal conductivity are presented. Three different levels of the average relative density of the material are considered, characterized by the respective expectation value $E(\bar{\rho})$. The corresponding probability density distributions f are presented in Fig. 8.

In the case of a low standard deviation $\sigma(\bar{\rho}) = 0.004$ and thus an insignificant scatter of the relative density, the scatter in the effective properties $\bar{E}$, $\bar{v}$, $\bar{\tau}_y$ and $\bar{\lambda}$ is caused solely by the scatter in the microstructural geometry and the uncertainty of the cell size distribution. With increasing standard deviation $\sigma(\bar{\rho})$, the scatter in the local relative density of the material increases. Consequently, the scatter to be expected in the effective properties increases, resulting in less steep increases of the corresponding probability functions F in Fig. 7 as well as wider ranges with a non-zero probability density f of the respective effective material properties (Fig. 8). Especially for the lowest considered expectation value $E(\bar{\rho}) = 0.1$, strongly asymmetric distributions of the probability density develop. Hence, a characterization of the scatter in the effective material properties in terms of the basic stochastic parameters E and σ alone without the explicit analysis of the corresponding probability distribution might be insufficient.

An interesting effect to be observed in Figs. 7 and 8 is the fact that the amount of uncertainty in the relative density $\bar{\rho}$ does not only affect the standard deviation of the effective properties but in some cases their median (and expectation) values as well. For an average relative density of $\bar{\rho} = 0.15$, the accumulated probability of $F = 0.5$ for the effective Young's modulus $\bar{E}/E_0$, the effective yield stress $\bar{\tau}_y/\tau_{y0}$ and the effective thermal conductivity $\bar{\lambda}/\lambda_0$ is reached at almost identical values of the respective effective properties, irrespectively of the scatter $\sigma(\bar{\rho})$ in the relative density. For $E(\bar{\rho}) = 0.2$ an increasing standard deviation $\sigma(\bar{\rho})$ and thus an increasing scatter in the local relative density of the material results in increasing median values of the respective effective material constant. For the less dense material with $E(\bar{\rho}) = 0.1$, the opposite effect is observed as the median effective properties decrease with increasing uncertainty in the local relative density $\bar{\rho}$.

The dependence of the mean values E and standard deviations σ of the effective material constants on the uncertainty in the local relative density in terms of the standard deviation $\sigma(\bar{\rho})$ is evaluated in more detail in Fig. 9. Black lines are related to the
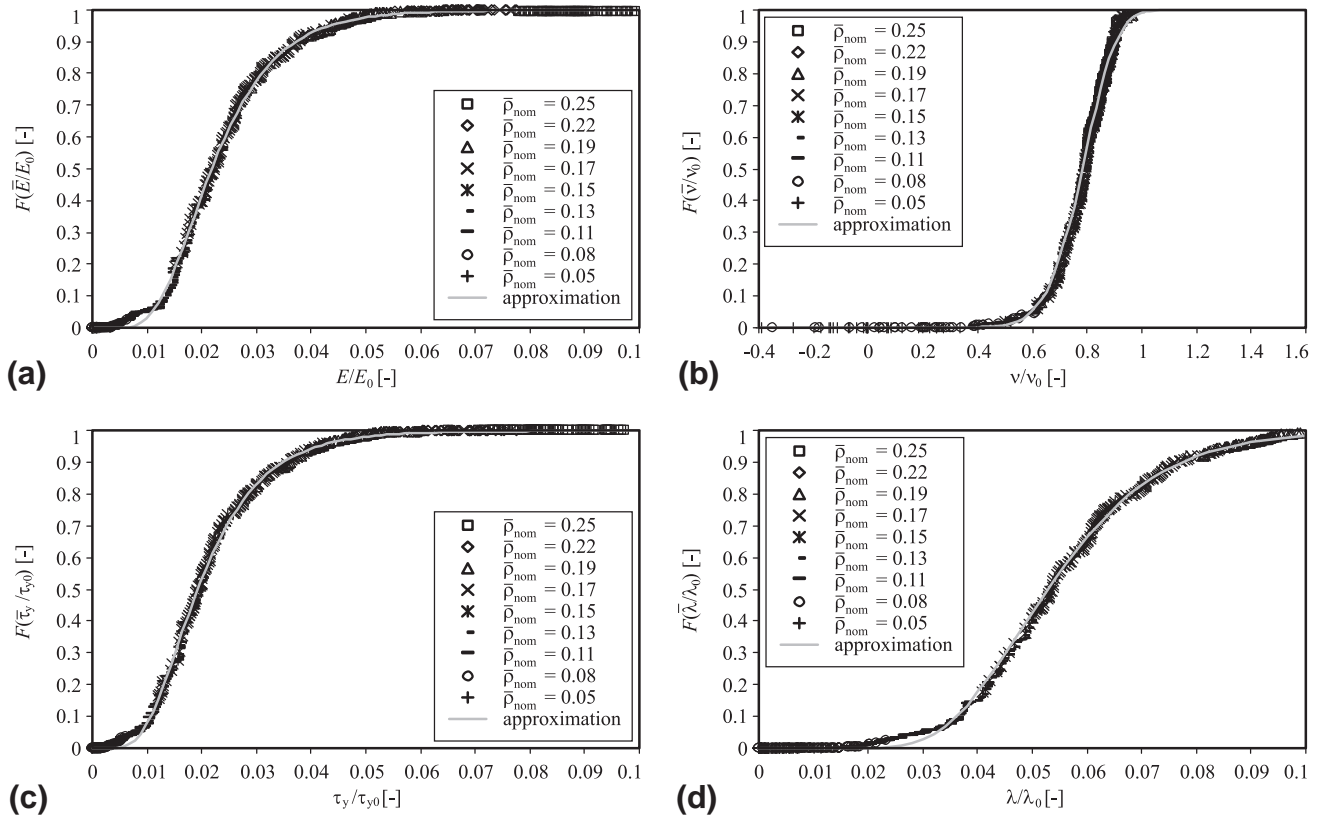
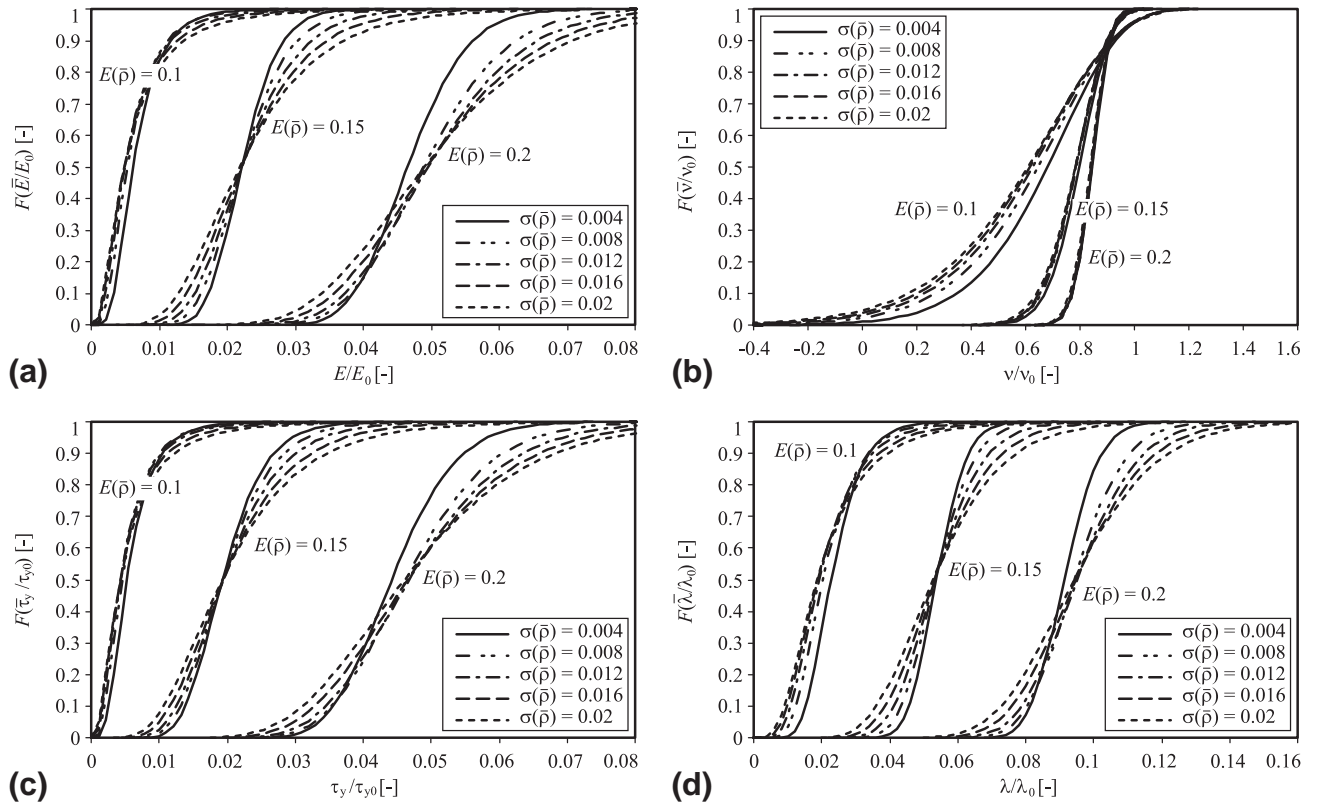**Fig. 6.** Stochastic evaluation of the numerical data base.

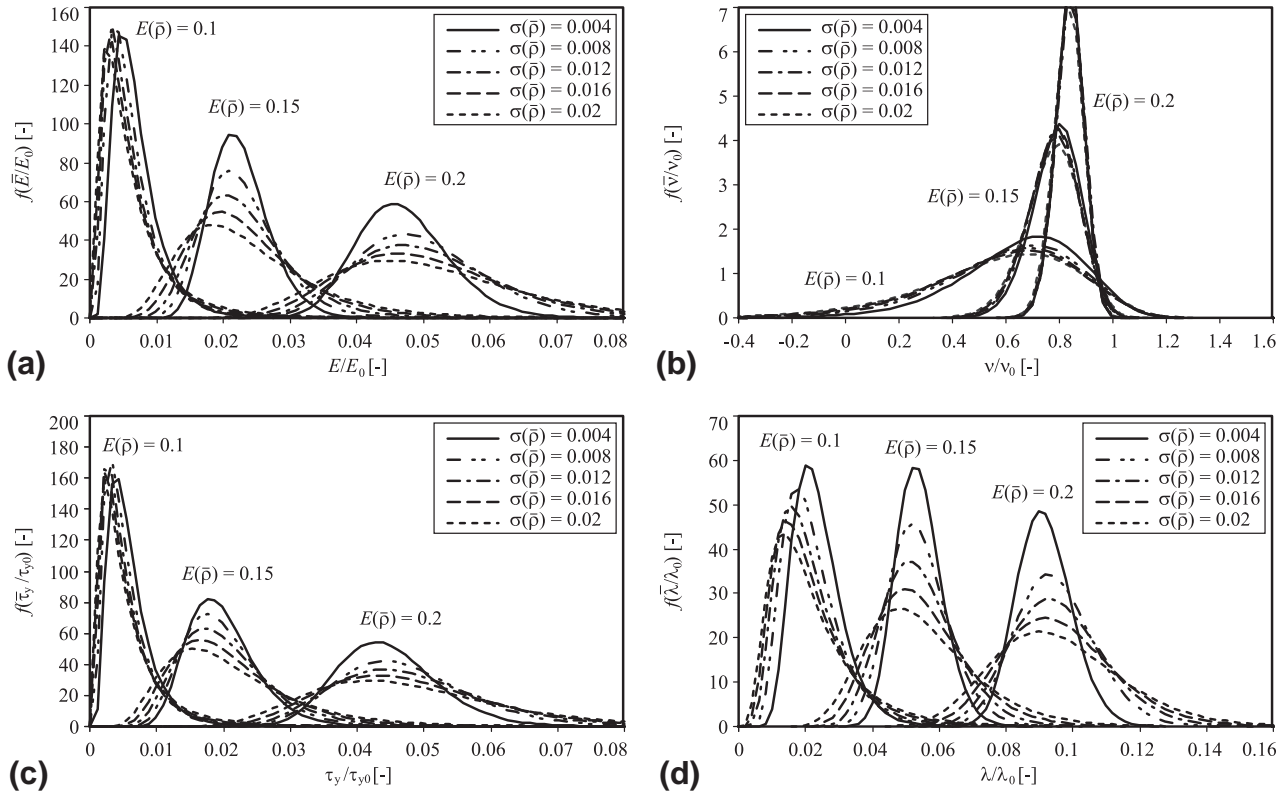**Fig. 7.** Effect of the uncertainty in the relative density, probability distributions.

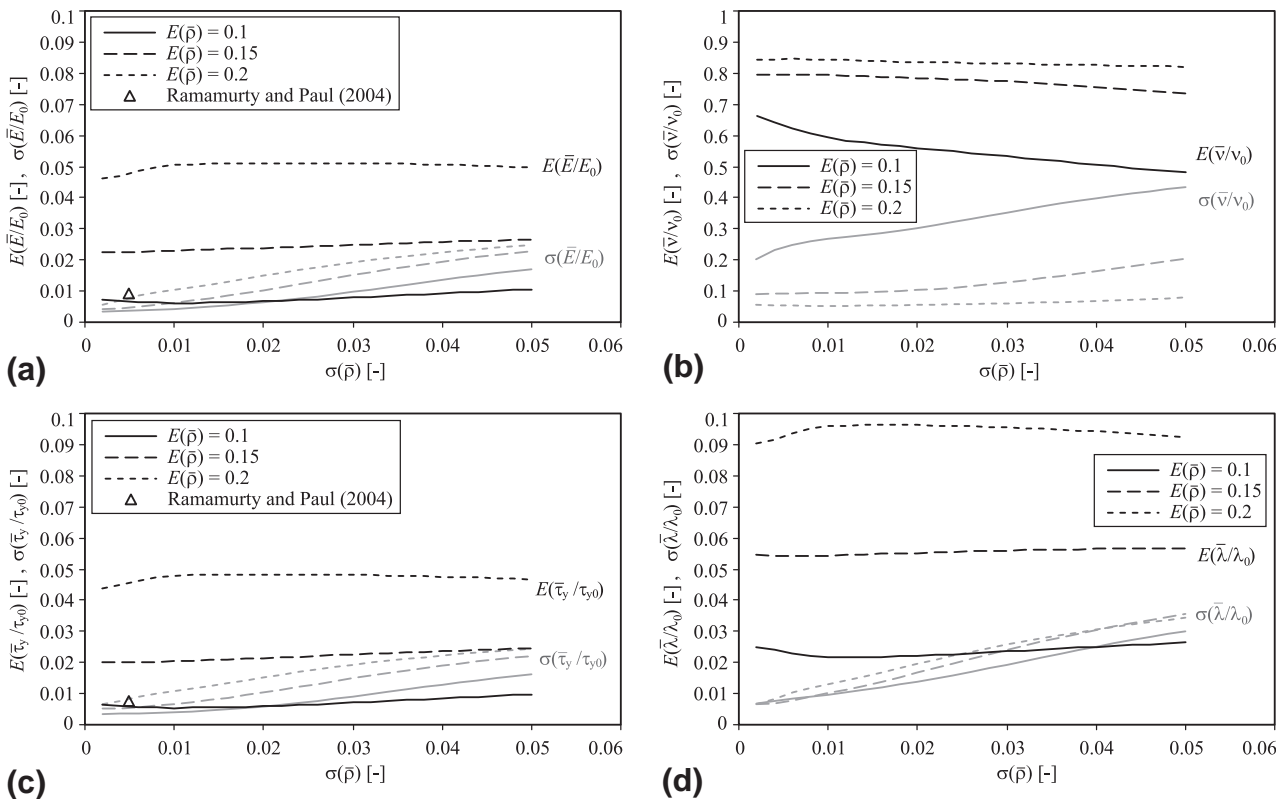**Fig. 8.** Effect of the uncertainty in the relative density, probability density distributions.

Fig. 9. Effect of the uncertainty in the relative density.

expectation value whereas the standard deviations are represented with gray lines. In case of the normalized effective Young's modulus $\overline{E}/E_0$, the normalized effective yield stress $\overline{\tau}_y/\tau_{y0}$ and the normalized effective thermal conductivity $\overline{\lambda}/\lambda_0$, the above mentioned effect of an increase in the mean effective properties for increasing scatter in the local relative density $\overline{\rho}$ is observed in the initial range of the standard deviation $\sigma(\overline{\rho})$ only (see Figs. 9(a), (c) and (d)). For a scatter in the relative density beyond $\sigma(\overline{\rho}) = 0.02$, the reverse effect is observed, although the significance in both ranges is limited. The strongest effect of the density scatter on an effective material constant is observed for the normalized effective Poisson's ratio $\overline{\nu}/\nu_0$ at the smallest mean relative density ($E(\overline{\rho}) = 0.1$, see Fig. 9(b)). The mean normalized effective Poisson's ratio decreases from approximately 0.66 at $\sigma(\overline{\rho}) = 0.004$ to 0.48 at $\sigma(\overline{\rho}) = 0.05$. For the uncertainties in the effective properties characterized by their standard deviations σ, in all cases monotonously increasing uncertainties are obtained with increasing uncertainty $\sigma(\overline{\rho})$ of the local relative density (see Fig. 9).

A comparison of the statistical means $E(\overline{E}/E_0)$ and $E(\overline{\tau}_y/\tau_{y0})$ of the effective Young's modulus and the effective yield stress with the experimental data by Ramamurty and Paul (2004) on an ALPO-RAS aluminum foam with a mean relative density of slightly less than $\overline{\rho} = 0.1$ yields a rather good agreement. The numerical results for $\overline{\rho} = 0.1$ at the respective standard deviation $\sigma(\overline{\rho})$ underpredict the experimental observations only slightly.

4.2. Effect of the sample size

In experimental investigations, the scatter in the effctive stiffness and transport properties in general strongly depends on the specimen size. Larger scatter is determined when using smaller specimens. The reason is the self-averaging effect of the material. In a similar manner, the effective properties determined by the numerical scheme proposed in the present study depend on the size of the testing volume elements employed. A simple method to quantify the expected effect based on the available raw data base in Fig. 4 consists in a re-combination of two or more raw data points based on testing volume elements with the same nominal microstructural properties. For these ensembles, the effective material constants are determined as the averages of the results from the individual testing volume element analyses. Subsequently, the stochastic evaluation is performed based on the ensemble averages instead of the individual results. By means of this procedure, the scatter in the effective constants to be expected when using testing volume elements with more than 20 cells can be estimated.

Based on this idea, a stochastic evaluation of the effective material properties is performed using samples consisting of a single testing volume element as well as ensembles of up to 16 testing volume elements and thus samples containing 20 up to 320 cells. In Fig. 10, the results for the standard deviation of the normalized elastic constants $\overline{E}/E_0$ and $\overline{\nu}/\nu_0$, the normalized yield stress $\overline{\tau}_y/\tau_{y0}$ and the normalized thermal conductivity $\overline{\lambda}/\lambda_0$ are presented in dependence on the number n_c of cells in the ensembles. For all four effective material constants investigated, increasing sample sizes result in decreasing uncertainties characterized by a decreasing standard deviation σ of the effective properties.

For comparison, the standard deviations of the normalized effective Young's modulus as well as the normalized yield stress derived from the experimental data presented by Ramamurty and Paul (2004) are added. In this context, the number of pores in the tested specimens is estimated from the average pore size. Again, the result for the elastic modulus does not incorporate the correction procedure for the specimen length suggested in Ramamurty and Paul's original contribution (Ramamurty and Paul, 2004). The scatter predicted by the present numerical scheme for

the effective Young's modulus is found in a good agreement with the experimental results on an aluminum foam with a scatter in the relative density of approximately $\sigma(\overline{\rho}) = 0.005$. For the scatter to be expected in the effective yield stress, a comparison of the experimental and numerical data is difficult since Ramamurty and Paul (2004) define the yield stress as the peak stress preceding the stress plateau in uniaxial compression whereas a definition in terms of the 0.2% offset stress is used in the present investigation. Since the plateau stress and quantities related to it are expected not to be affected by the scatter in the elastic properties, a less distinct scatter has to be expected for the yield stress determined in terms of the plateau stress compared to the yield stress defined as the stress at a 0.2% offset limit close to the elastic range. Since this quantity is expected to be affected by the elastic properties and thus the scatter therein, both yield stress values might not be directly comparable, especially in terms of their uncertainty.

4.3. Effect of the cell size distribution

In all previous parametric studies, a similar cell size distribution has been assumed. The size distribution is of the logarithmic normal type (12) with an uncertain shape parameter σ_{csz}. The expectation value and the standard deviation of the uncertain shape parameter were assumed to be $E(\sigma_{csz}) = 0.3$ and $\sigma(\sigma_{csz}) = 0.1$ respectively, both normalized with the volume of the testing volume elements.

In a final investigation, the effect of the uncertainty in the local cell size distribution on the expectation value and the standard deviation of the effective material properties $\overline{E}$, $\overline{\nu}$, $\overline{\tau}_y$ and $\overline{\lambda}$ is studied. The results are presented in Fig. 11, where three different expectation values $E(\sigma_{csz})$ of the shape parameter for the cell size distribution are considered. The lowest considered expectation value of $E(\sigma_{csz}) = 0.2$ is related to a slightly disordered microstructure whereas the intermediate value of $E(\sigma_{csz}) = 0.3$ and the highest value of $E(\sigma_{csz}) = 0.4$ characterize moderately and distinctively disordered microstructures respectively. In all three cases, the standard deviation $\sigma(\sigma_{csz})$ is varied over the interval [0.01, 0.2] covering the range from certain to highly uncertain shape parameters σ_{csz} of the local cell size distribution (see Fig. 3). The expectation value of the relative density and the corresponding standard deviation are kept constant at $E(\overline{\rho}) = 0.15$ and $\sigma(\overline{\rho}) = 0.01$ respectively.

With respect to the expectation values $E(\overline{E}/E_0), E(\overline{\nu}/\nu_0), E(\overline{\tau}_y/\tau_{y0})$ and $E(\overline{\lambda}/\lambda_0)$ of the effective material properties, no significant effect of an uncertainty in the cell size distribution is observed. Equivalent results for all four effective properties are obtained irrespectively of the expectation value $E(\sigma_{csz})$ of the shape parameter of the cell size distribution and its standard deviation $\sigma(\sigma_{csz})$. Due to the limited numerical data base, some slight differences between the curves for the three different expectation values $E(\sigma_{csz})$ develop at low standard deviations $\sigma(\sigma_{csz})$. In these cases, only narrow scatter bands of the shape parameter σ_{csz} of the cell size distribution are assumed. Hence, the results for the effective properties depend solely on the results based on the testing volume element analyses with a shape parameter σ_{csz} of the cell size distribution equal to the respective assumed expectation value $E(\sigma_{csz})$. With increasing $\sigma(\sigma_{csz})$ and thus an increasing scatter band width for the parameter σ_{csz}, an increasing number of testing volume element analyses affects the statistical evaluation with non-negligible individual probablity p. Hence, smoother probability distributions are obtained for larger $\sigma(\sigma_{csz})$ resulting in more stable results for the expectation values of the effective properties.

Qualitatively similar results are obtained for the effect of the standard deviation $\sigma(\sigma_{csz})$ of the shape parameter σ_{csz} of the cell size distribution on the standard deviation of the effective material
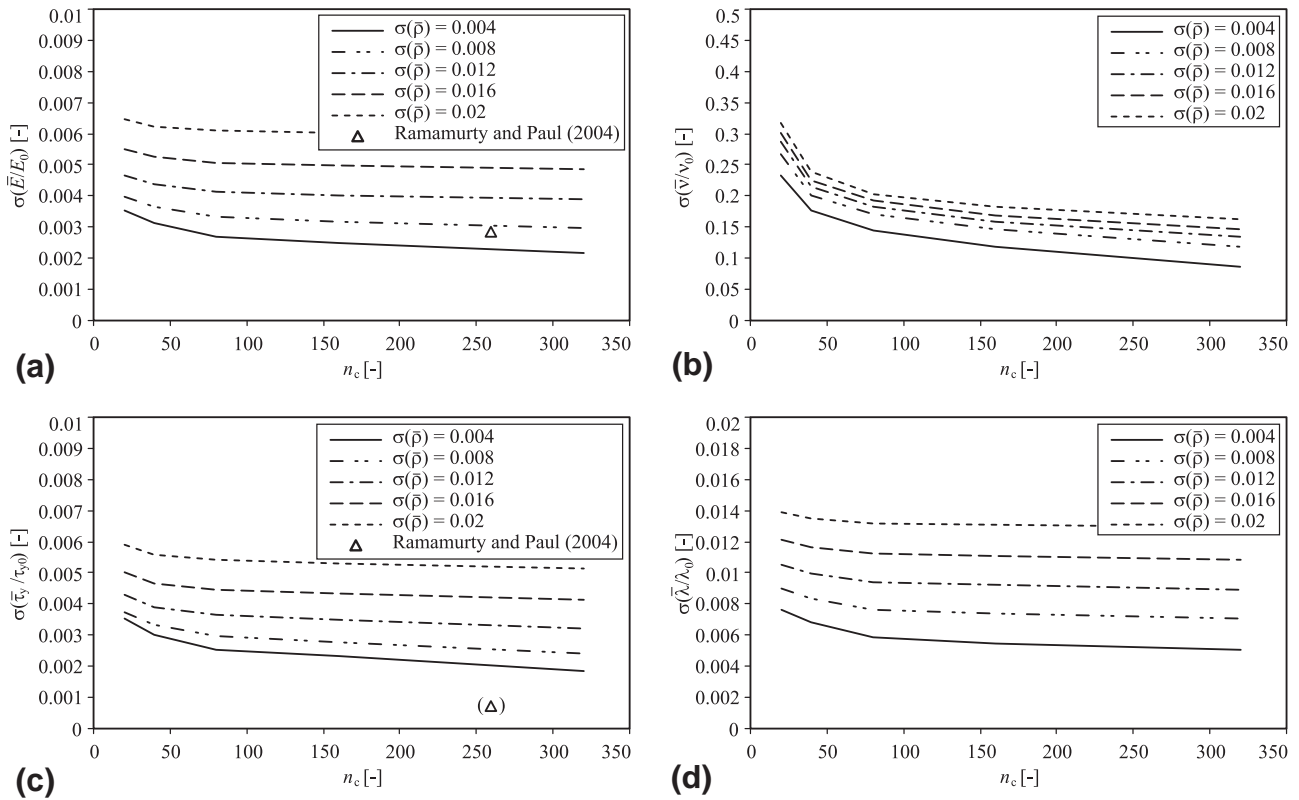
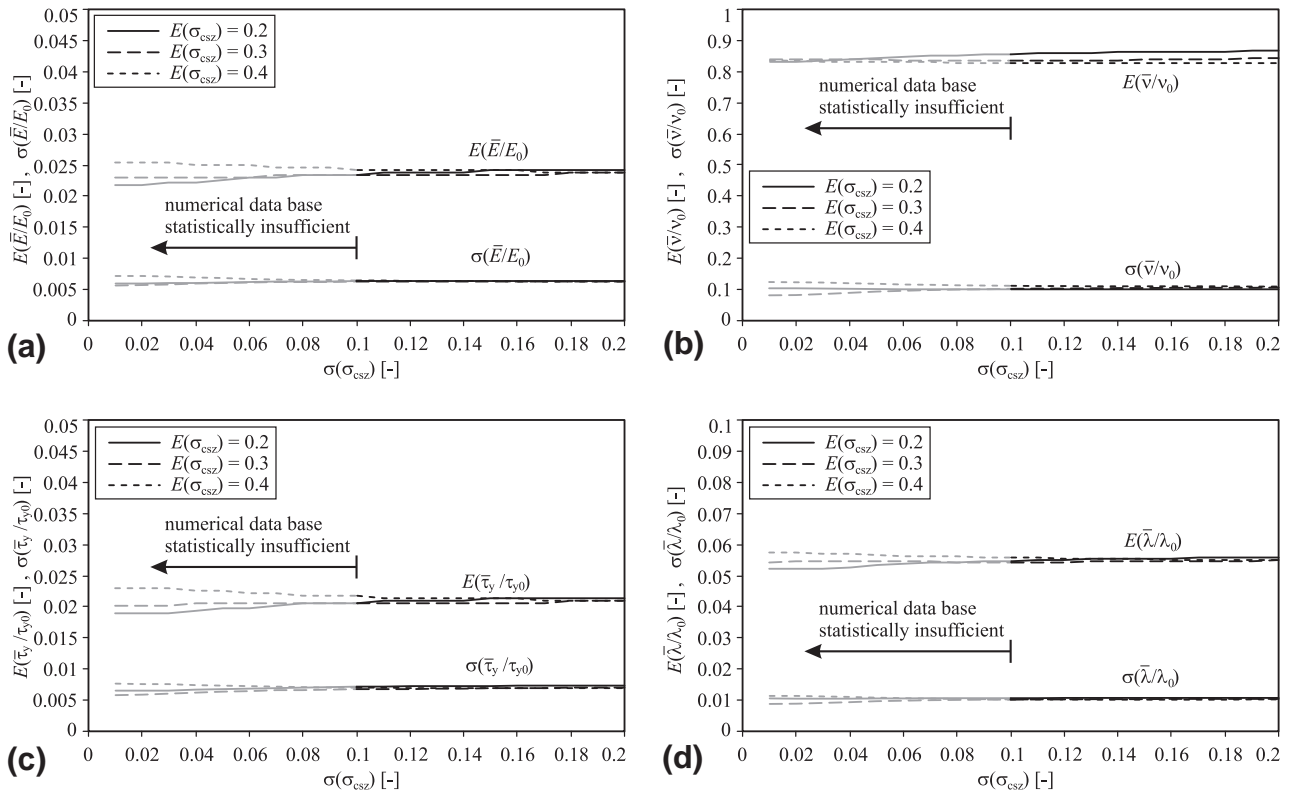Fig. 10. Effect of the testing volume element size.

Fig. 11. Effect of the cell size distribution.

properties. Whereas no significant effect is observed for $\sigma(\sigma_{csz}) > 0.1$, numerically unstable results are obtained for lower

$\sigma(\sigma_{csz})$ due to the statistically insufficient numerical data base in this range. The insufficiency is caused by the limitation of the sto-

chastic evaluation to the testing volume element analyses based on cell size distributions with a shape parameter σ_{csz} equal to the assumed expectation value $E(\sigma_{csz})$.

5. Conclusion

The objective of the present study is the probabilistic numerical analysis of the effective properties of three-dimensional porous solids. For this purpose, a stochastic homogenization developed previously for the analysis of two-dimensional honeycombs is extended to the three-dimensional case. The procedure is based on the multiple homogenization of testing volume elements with prescribed values of the uncertain constitutive parameters defining the microstructure. The results of the testing volume element analyses are weighted with the individual probabilities for occurrence of the underlying microstructural case. As basic uncertain microstructural constitutive properties, the local relative density, the cell size distribution, the spatial orientation of the testing volume element and the microstructural geometry are considered. The scatter and uncertainty of these properties is quantified in terms of their probability distributions.

In the present study, logarithmic normal distributions are assumed for the relative density and the shape parameter of the cell size distribution whereas homogeneous distributions are assumed for the orientation of the testing volume elements in space as well as for the topology of the randomly generated microstructures. For the homogenization itself, a strain energy based approach is utilized, assuming the mesoscopic equivalence of the microstructure and the quasi-homogeneous effective medium, if equal average strain energy density states are obtained provided that the testing volume elements for the microstructure and the effective medium are deformed in deformation states, which are equal in a volume average sense.

In a number of parametric studies on an aluminum foam, the local relative density proves to be the most important stochastic variable. The microstructural scatter caused by the uncertainty of the local relative density does not only affect the scatter in the effective properties but may also affect the median or expectation values respectively. For the local cell size distribution, significant effects are observed neither in the scatter of the effective properties nor in their expectation values. Nevertheless, it has to be considered that for real porous materials, especially for foams, the cell size might be correlated with the local relative density. This correlation is caused by the fact that for low density solid foams the cell wall thickness for small and large cells is in many cases similar. Hence, zones with small pores feature a larger density of cell walls and thus a larger local material density than areas with large pores.

The parametric studies reveal that the stochastic homogenization scheme proposed in the present study enables a numerically efficient prediction of the uncertainty in the effective properties from the known uncertainty in the microstructural properties of the material. Nevertheless, care has to be taken in order to assure the use of a sufficiently large numerical data base, since the significant part of the total numerical data base might shrink significantly in the case of narrow scatter band widths of the uncertain variables. Therefore, a sufficiently fine resolution of the ranges for the basic uncertain microstructural properties is necessary in order to obtain convergent results based on a statistically sufficient numerical data base.

References

Bishop, J.F.W., Hill, R., 1951. A theory of the plastic distortion of a polycrystalline aggregate under combined stress. Phil. Mag. 42, 414–427.

Blazy, J.S., Marie-Louise, A., Forest, S., Chastel, Y., Pineau, A., Awade, A., Grolleron, C., Moussy, F., 2004. Deformation and fracture of aluminium foams under proportional and multi-axial loading: statistical analysis and size effect. Int. J. Mech. Sci. 46, 217–244.

Christensen, R.M., 1987. Sufficient symmetry conditions for isotropy of the elastic moduli tensor. J. Appl. Mech. 54, 772–777.

Cuitiño, A.M., Zheng, S., 2003. Taylor averaging on heterogeneous foams. J. Compos. Mat. 37, 701–713.

Fortes, M.A., Ashby, M.F., 1999. The effect of non-uniformity on the in-plane modulus of honeycombs. Acta Mater. 47, 3469–3473.

Gan, Y.X., Chen, C., Shen, Y.P., 2005. Three-dimensional modeling of the mechanical property of linearly elastic open cell foams. Int. J. Solids Struct. 42, 6628–6642.

Gent, A.N., Thomas, A.G., 1963. Mechanics of foamed elastic materials. Rubber Chem. Techn. 36, 597–610.

Gibson, L.J., Ashby, M.F., 1997. Cellular Solids – Structure and Properties. Pergamon Press, Oxford.

Hardenacke, V., Hohe, J., 2009. Local probabilistic homogenization of two-dimensional model foams accounting for micro structural disorder. Int. J. Solids Struct. 46, 989–1006.

Hohe, J., Becker, W., 2001. An energetic homogenization procedure for the elastic properties of general cellular sandwich cores. Compos. B 32, 185–197.

Hohe, J., Becker, W., 2005. A probabilistic approach to the numerical homogenization of irregular solid foams in the finite strain regime. Int. J. Solids Struct. 42, 3549–3569.

Huyse, L., Maes, M.A., 2001. Random field modeling of elastic properties using homogenization. J. Eng. Mech. 127, 27–36.

Kanaun, S., Tkachenko, O., 2006. Mechanical properties of open-cell foams: simulations by Laguerre tesselation procedure. Int. J. Frac. 140, 303–312.

Li, K., Gao, X.L., Subhash, G., 2006. Effects of cell shape and strut cross-sectional area variations on the elastc properties of three-dimensional open-cell foams. J. Mech. Phys. Solids 54, 783–806.

McCullough, K.Y.G., Fleck, N.A., Ashby, M.F., 1999. Uniaxial stress–strain behaviour of aluminium alloy foams. Acta Mater. 47, 2323–2330.

Ramamurty, U., Paul, A., 2004. Variability in mechanical properties of a metal foam. Acta Mat. 52, 869–876.

Roberts, A.P., Garboczi, E.J., 2002. Elastic properties of model random three-dimensional open-cell solids. J. Mech. Phys. Solids 50, 33–55.

Ruan, D., Lu, G., Chen, F.L., Siores, E., 2002. Compressive behaviour of aluminium foams at low and medium strain rates. Compos. Struct. 57, 331–336.

Ruan, D., Lu, G., Ong, L.S., Wang, B., 2007. Triaxial compression of aluminium foams. Compos. Sci. Tech. 67, 1218–1234.

Schraad, M.W., Harlow, F.H., 2006. A stochastic constitutive model for disordered cellular materials: finite-strain uni-axial compression. Int. J. Solids Struct. 43, 3542–3568.

Shulmeister, V., van der Burg, M.W.D., van der Giessen, E., Marissen, R., 1998. A numerical study of large deformation of low-density elastomeric open-cell foams. Mech. Mat. 30, 125–140.

Solórzano, E., Rodríguez-Pérez, M.A., Reglero, J.A., de Saja, J.A., 2007. Density gradients in aluminium foams: Characterisation by computed tomography and measurements of the effective thermal conductivity. J. Mat. Sci. 42, 2557–2564.

Thomson, W., Kelvin, Lord, 1887. On the division of space with minimum partitional area. Phil. Mag. 24, 503–514.

van der Burg, M.W.D., Shulmeister, V., van der Giessen, E., Marissen, R., 1997. On the linear elastic properties of regular and random open-cell foam models. J. Cell. Plastics 33, 31–54.

Weaire, D., Phelan, R., 1994. A counter-example to Kelvin's conjecture on minimal surfaces. Phil. Mag. Let. 69, 107–110.

Zhu, H.X., Windle, A.H., 2002. Effects of cell irregularity on the high strain compression of open-cell foams. Acta Mater. 50, 1041–1052.

Zhu, H.X., Hobdell, J.R., Windle, A.H., 2000. Effects of cell irregularity on the elastic properties of open-cell foams. Acta Mater. 48, 4893–4900.